Supporting Information

Selective Nitrogen Doping on Porous Hard Carbons Using Polymer Dopants for High-Performance Fuel Cells

Yoon-A Jang [a, †], Daehyeon Seo [b, †], Taewook Kim [a, c], Jae Hyun Park [d], Youngkyu Bae [d], Gilhwan Lee [d], Young Jun Lee [b, *], Chan Ho Park [a, *]

†These authors contributed equally to this work.

[a] Department of Chemical, Biological, and Battery Engineering, Gachon University, 1342 Seongnam-daero, Sujeong-gu, Seongnam-si, Gyeonggi-do, 13120, Republic of Korea

* E-mail: chhopark@gachon.ac.kr (C. H. P.)

[b] Carbon Composite Materials Research Center, Korea Institute of Science and Technology, 92 Chudong-ro, Bongdong-eup, Wanju-gun, Jeonbuk, 55324, Republic of Korea

* E-mail: youngjunlee@kist.re.kr (Y. J. L.)

[c] Thin Film Materials Research Center, Korea Research Institute of Chemical Technology, 141 Gajeong-ro, Yuseong-gu, Daejeon, 34114, Republic of Korea

[d] The Carbon Studio, 4, Techno 2-ro, Yuseong-gu, Daejeon, Republic of Korea

Table of Contents

Supplementary Figures S1-S15

Supplementary Tables S1-S8

Table S1. Composition of PCC/P4VP complexes with different PCC-to-P4VP mass ratios.

Sample	PCC (wt.%)	P4VP (wt.%)	PCC:P4VP ratio (w/w)
PCC	100	0	
PCC/P4VP complex (10:1)	10	1	10:1
PCC/P4VP complex (20:1)	20	1	20:1

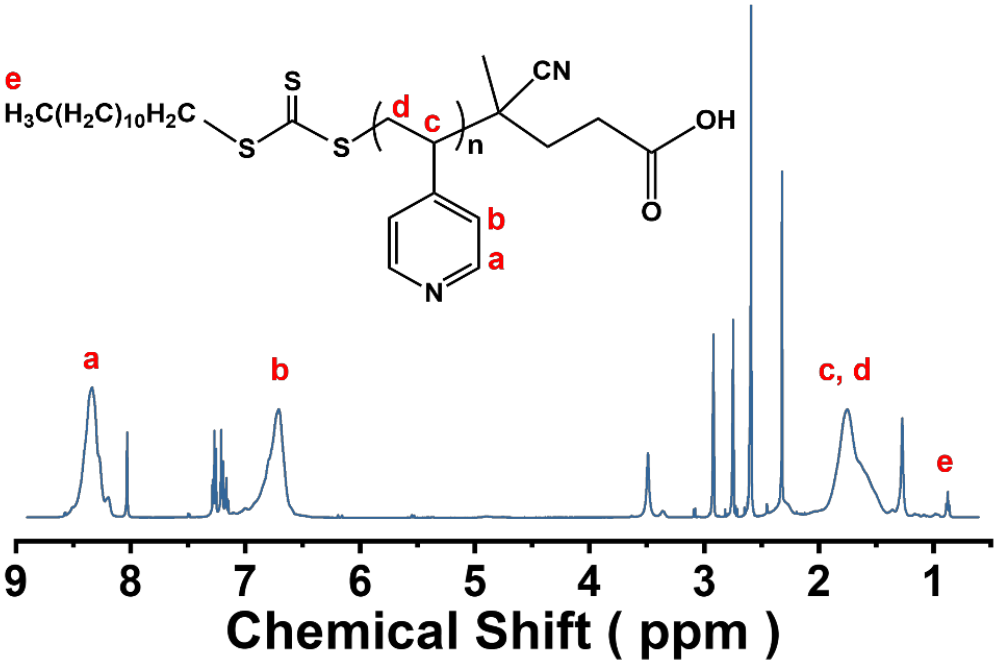

Fig. S1. ^{1}H NMR spectra of P4VP (M_n =12.3 kDa) in DMF-d_7 at room temperature.

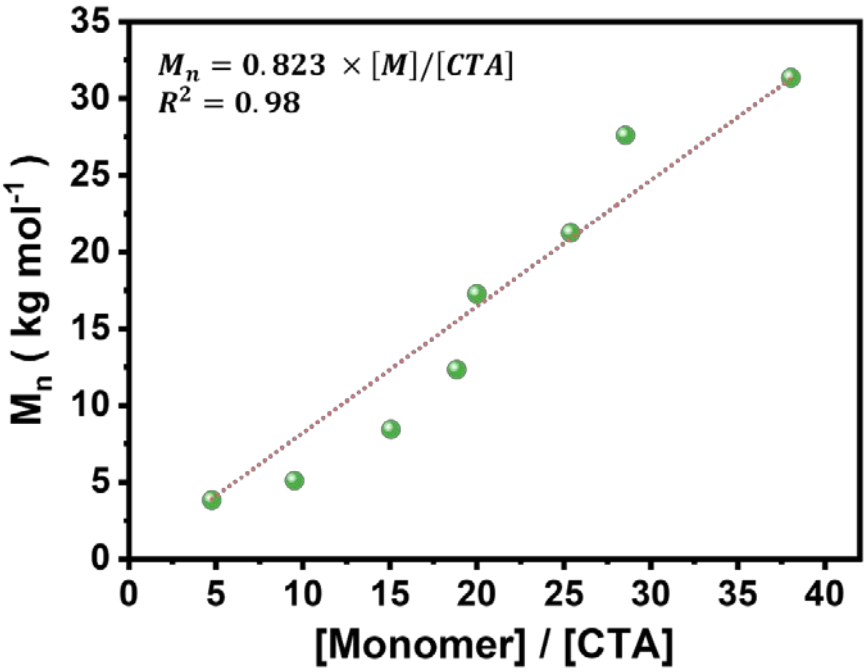

Fig. S2. M_n as a function of [Monomer]/[CTA] for P4VP synthesized via RAFT polymerization. M_n increases linearly with [M]/[CTA], following $M_n = 0.823 \times$ [M]/[CTA] (kg mol^{-1}, $R^2 = 0.98$).

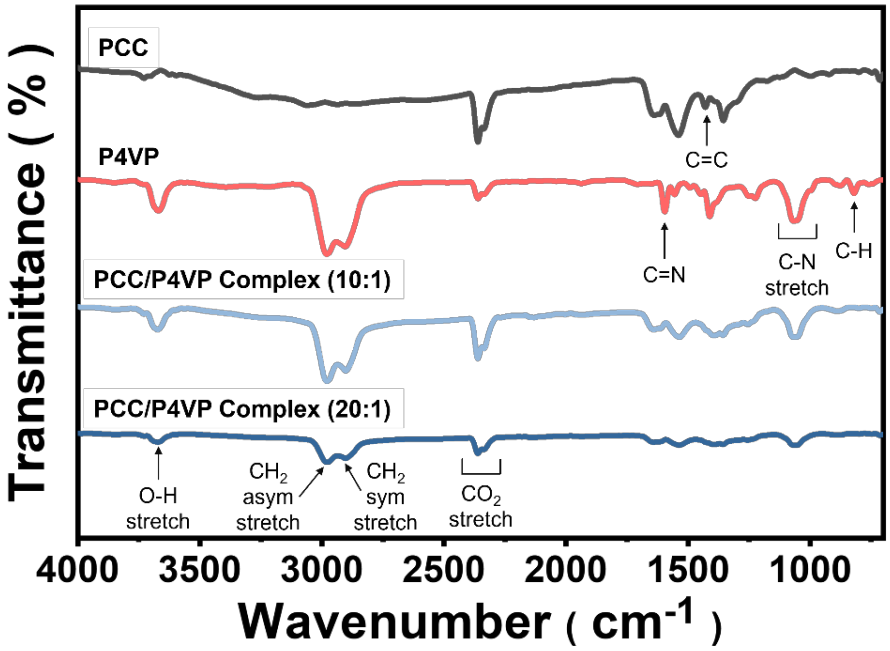

Fig. S3. FTIR spectra of PCC, P4VP, and PCC/P4VP complexes.

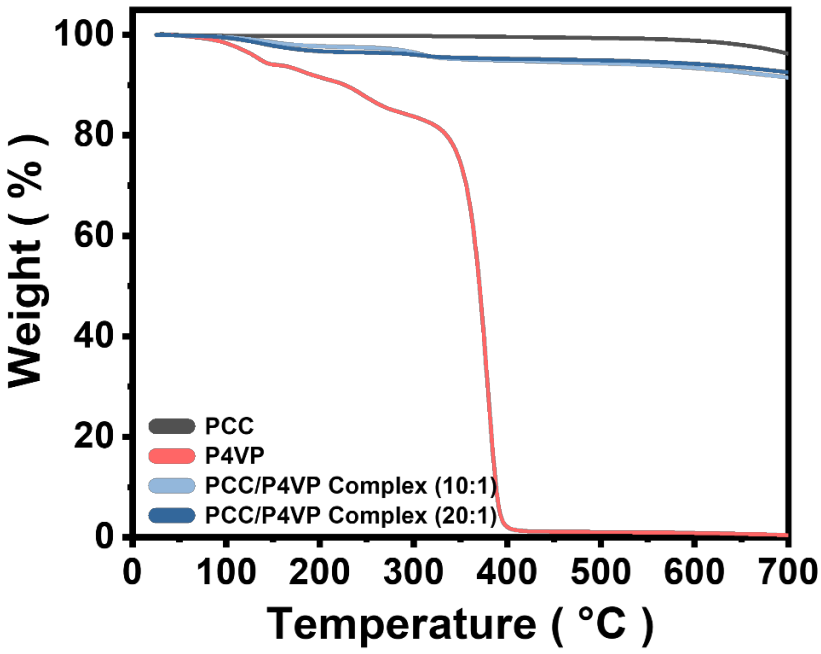

Fig. S4. TGA curves of PCC, P4VP, and PCC/P4VP complexes.

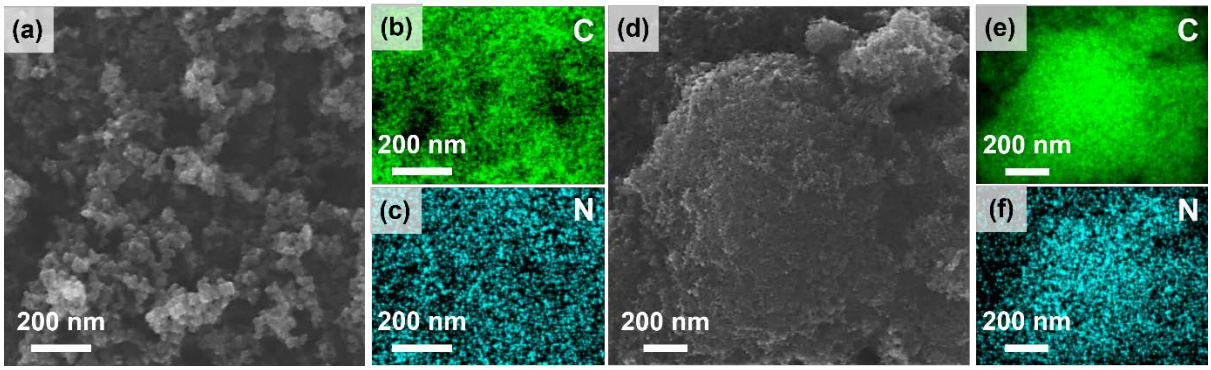

Fig. S5. SEM images of (a) PCC/P4VP complex (10:1) and (d) N-doped PCC (10:1). EDS mapping images of PCC/P4VP complex (10:1) and N-doped PCC (10:1), showing the distribution of (b, e) C (green) and (c, f) N (cyan).

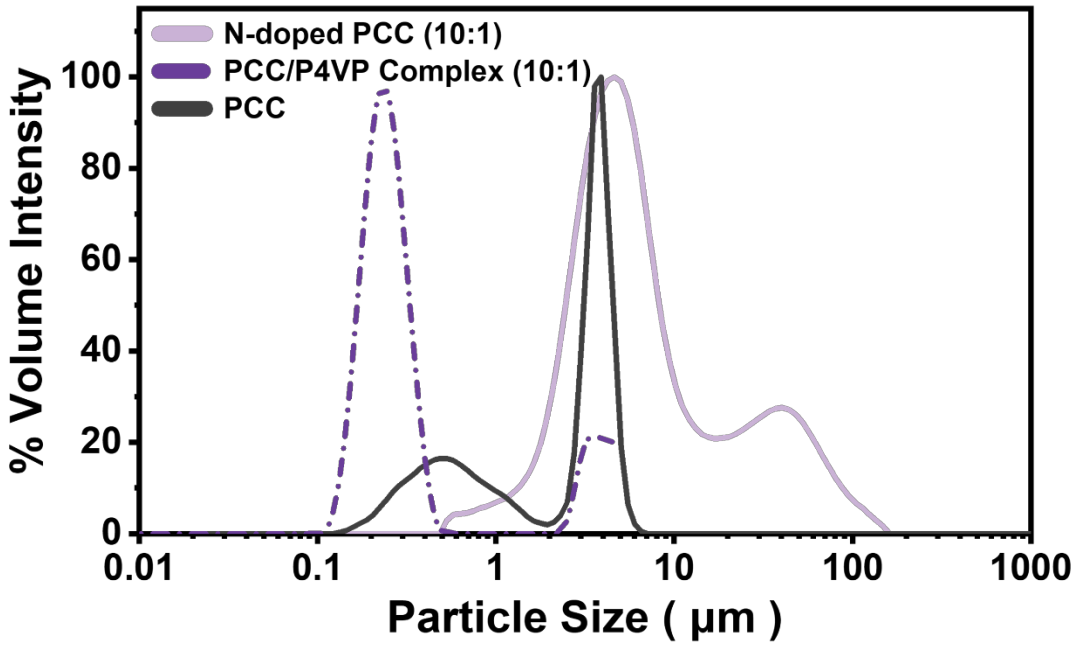

Fig. S6. Particle size distributions of PCC, PCC/P4VP complex (10:1), and N-doped PCC (10:1).

Table S2. Elemental compositions (atomic %) of N-doped PCCs, as determined by XPS.

Sample	C (at. %)	O (at. %)	N (at. %)
N-doped PCC (10:1)	97.81	0.52	1.68
N-doped PCC (20:1)	97.93	1.16	0.91

Table S3. Elemental compositions (atomic %) of pristine PCC and P4VP-assisted N-doped PCCs with different P4VP molecular weights.

No.	Sample	Sample Conditions			XPS-derived elemental composition		
		Synthesis method of P4VP	**P4VP M_n (kDa)**	**PCC:P4VP ratio (wt.%)**	**C (at. %)**	**O (at. %)**	**N (at. %)**
1	**PCC**	-	-	-	96.98	3.02	-
2	**N-doped PCCs**	RAFT polymerization	12	10:1	97.81	0.52	1.68
3		Commercial (purchased Sigma-Aldrich)	60		98.17	0.96	0.87

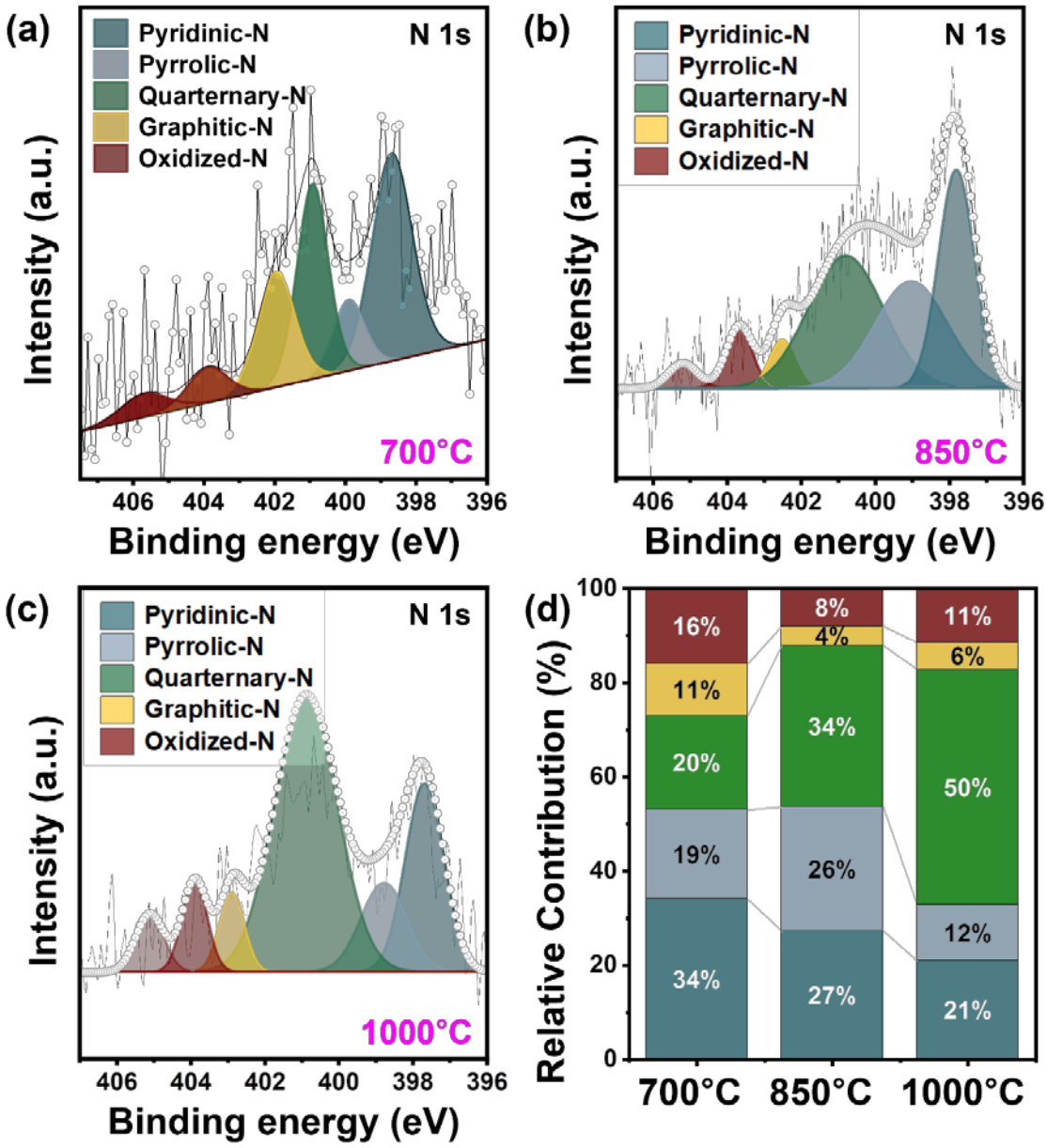

Fig. S7. High-resolution N 1s XPS spectra of P4VP-derived PCCs carbonized at (a) 700 ℃, (b) 850 ℃, and (c) 1000 ℃. (d) Relative contribution of N species (%) derived from N 1s deconvolution.

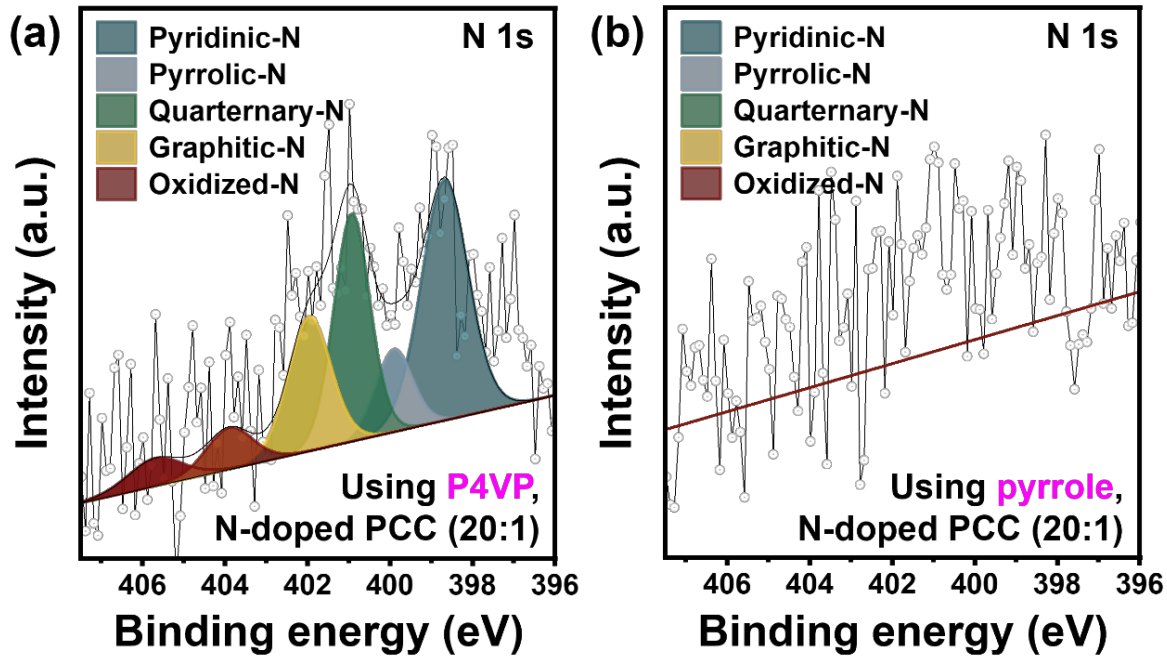

Fig. S8. High-resolution N 1s XPS spectra of N-doped PCC (20:1) obtained using (a) P4VP and (b) pyrrole as N sources.

Table S4. Textural properties of pristine PCC and N-doped PCCs.

Sample	BET SSA ($m^2 g^{-1}$)	Micro SSA by t-plot ($m^2 g^{-1}$)	Micro SSA ratio (%)	Pore Volume ($cm^3 g^{-1}$)	Average Pore Width (nm)
PCC	600.13	108.46	18.07	1.41	8.07
N-doped PCC (10:1)	446.51	58.81	13.17	1.47	9.68
N-doped PCC (20:1)	399.46	63.95	16.01	1.33	9.34

Table S5. Textural properties of A4, FB and N-doped A4, FB.

Sample	BET SSA ($m^2 g^{-1}$)	Micro SSA by t-plot ($m^2 g^{-1}$)	Micro SSA ratio (%)	Pore Volume ($cm^3 g^{-1}$)	Average Pore Width (nm)
A4	449.53	74.72	16.62	0.83	6.68
N-doped A4	328.28	42.96	13.09	0.83	10.11
FB	1100.66	151.13	13.73	1.91	6.74
N-doped FB	780.74	52.46	6.72	1.75	7.37

Table S6. Elemental compositions (atomic %) of A4, FB and N-doped A4, FB, as determined by XPS.

Sample	C (at. %)	O (at. %)	N (at. %)
A4	97.06	2.94	
N-doped A4	98.27	0.60	1.13
FB	97.43	2.57	
N-doped FB	97.89	1.10	1.01

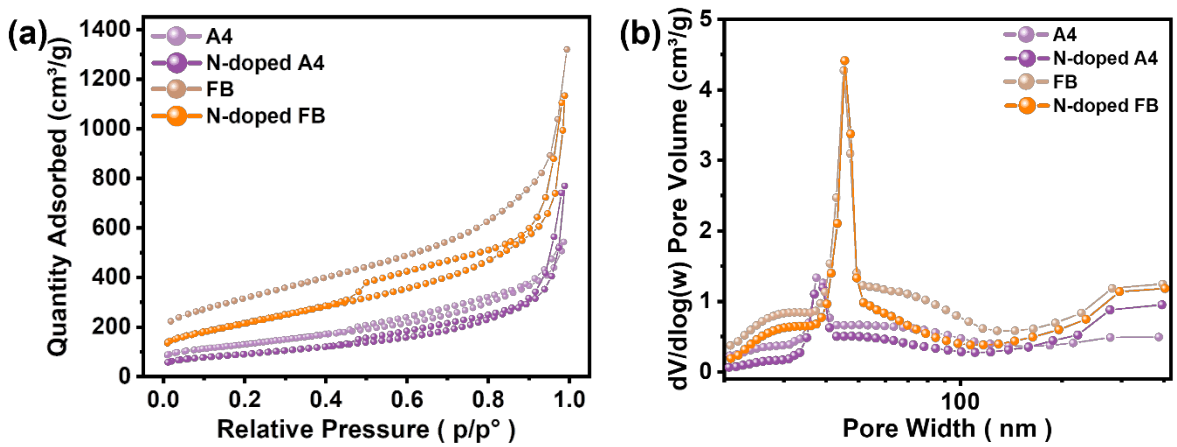

Fig. S9. Characterization of A4, FB, and N-doped A4, FB: (a) N_2-soprtion isotherms, and (b) pore size distribution curves obtained from BJH desorption analysis.

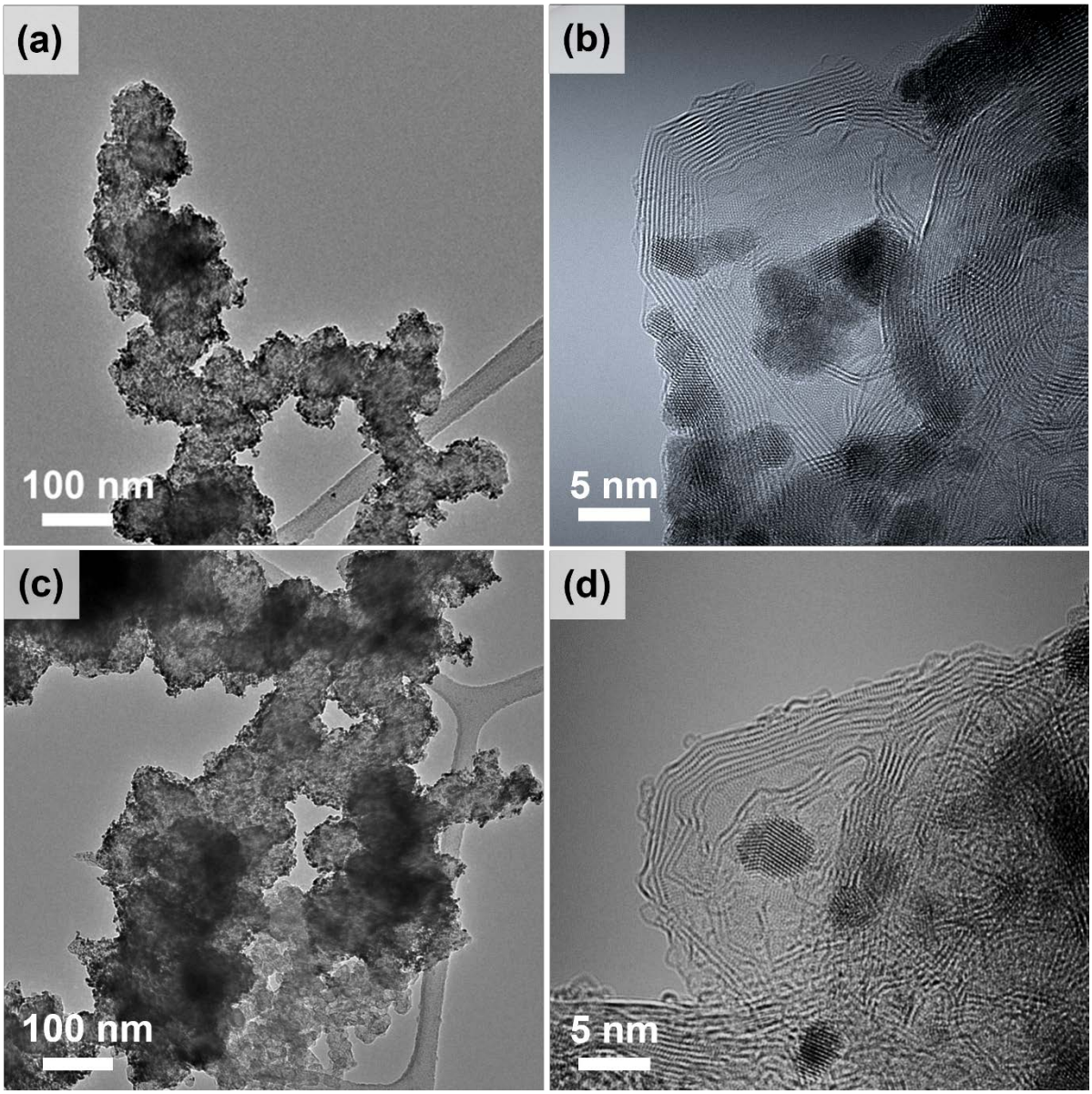

Fig. S10. TEM images of (a) Pt/N-doped PCC (10:1) and (c) Pt/N-doped PCC (20:1), along with HR-TEM images of (b) Pt/N-doped PCC (10:1) and (d) Pt/N-doped PCC (20:1).

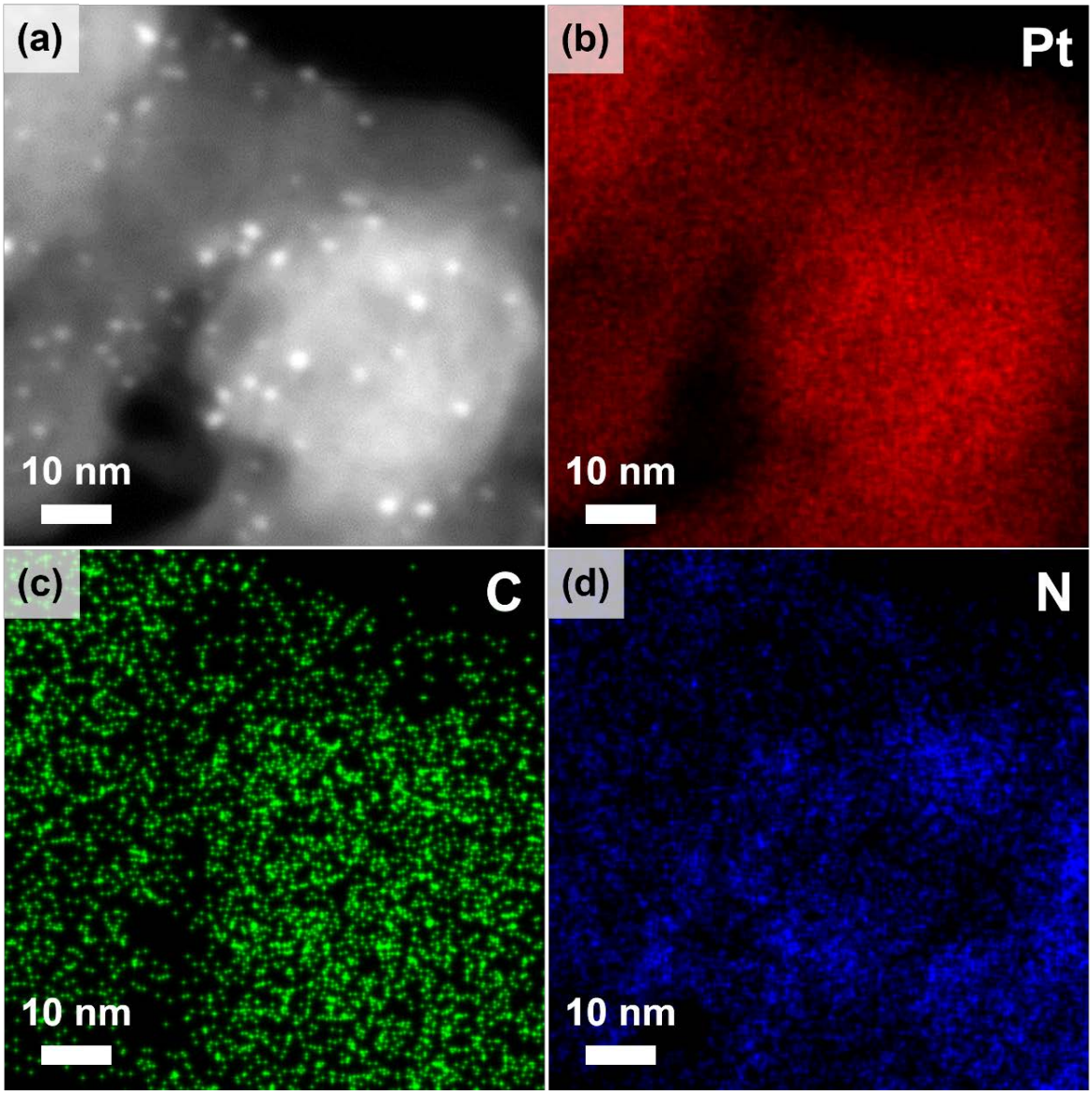

Fig. S11. STEM-HAADF image of (a) Pt/N-doped PCC (20:1) and corresponding EDS elemental maps showing (b) Pt (red), (c) C (green), and (d) N (blue) distributions.

Table S7. Elemental compositions (atomic %) of the synthesized Pt at N-doped PCCs, obtained from EDS analysis conducted using TEM.

Sample	C (at. %)	O (at. %)	N (at. %)	Pt (at. %)
Pt/N-doped PCC (10:1)	95.75	1.53	0.19	2.53
Pt/N-doped PCC (20:1)	95.06	1.26	0.48	3.20

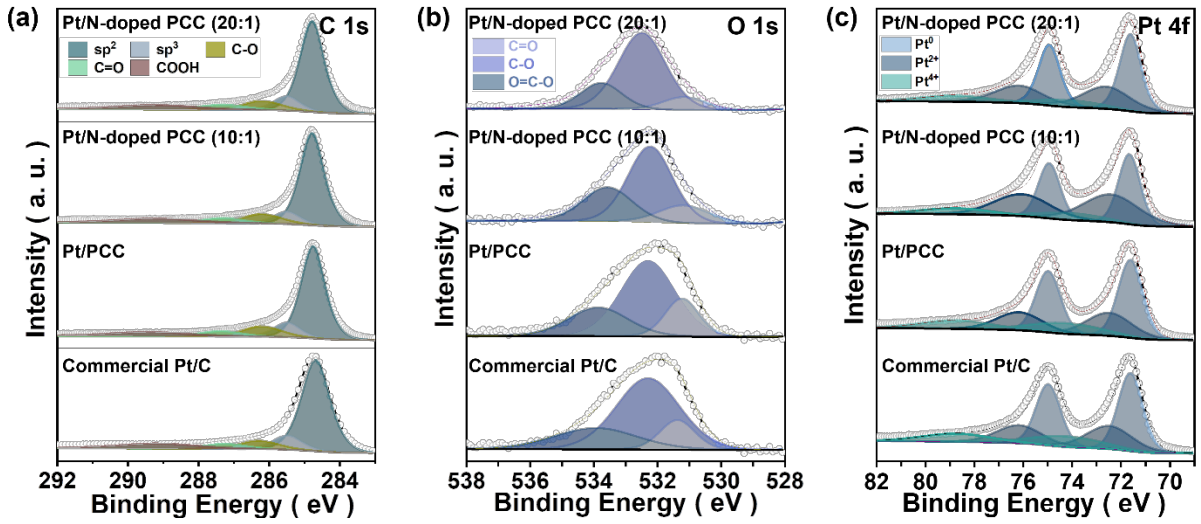

Fig. S12. High-resolution XPS spectra of commercial Pt/C, Pt/PCC, and Pt/N-doped PCCs: (a) C 1s, (b) O 1s, and (c) Pt 4f.

Table S8. Elemental compositions (atomic %) of Pt in commercial Pt/C and Pt/PCC-based catalysts obtained from XPS analysis.

Sample	Pt^0 (at. %)	Pt^{2+} (at. %)	Pt^{4+} (at. %)
Commercial Pt/C	51.9	38.7	9.4
Pt/PCC	69.7	24.1	6.2
Pt/N-doped PCC (10:1)	68.6	27.3	4.1
Pt/N-doped PCC (20:1)	65.2	27.5	7.3

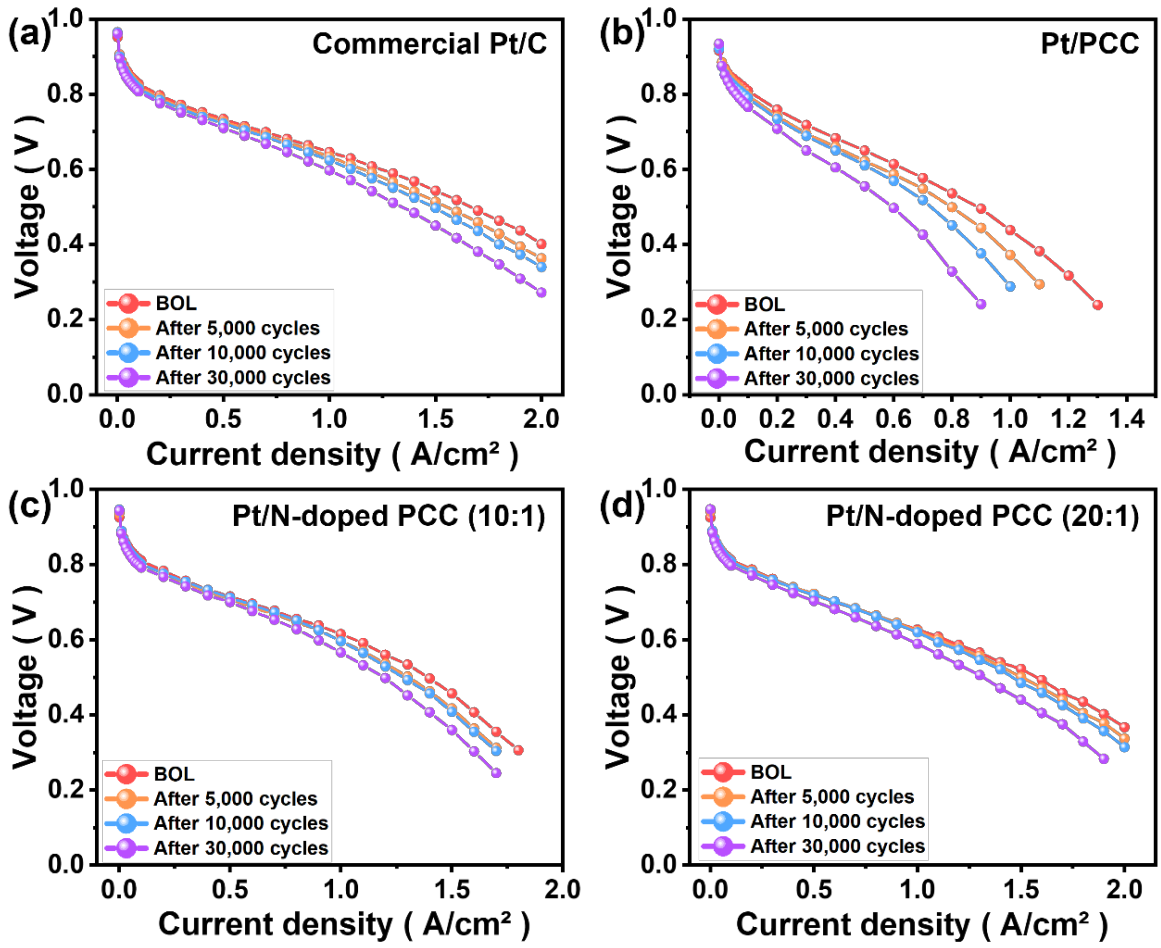

Fig. S13. I-V polarization curves of (a) commercial Pt/C, (b) Pt/PCC, (c) Pt/N-doped PCC (10:1), and (d) Pt/N-doped PCC (20:1). The curves are shown for BOL, after 5,000, after 10,000, and after 30,000 cycles under 40% RH.

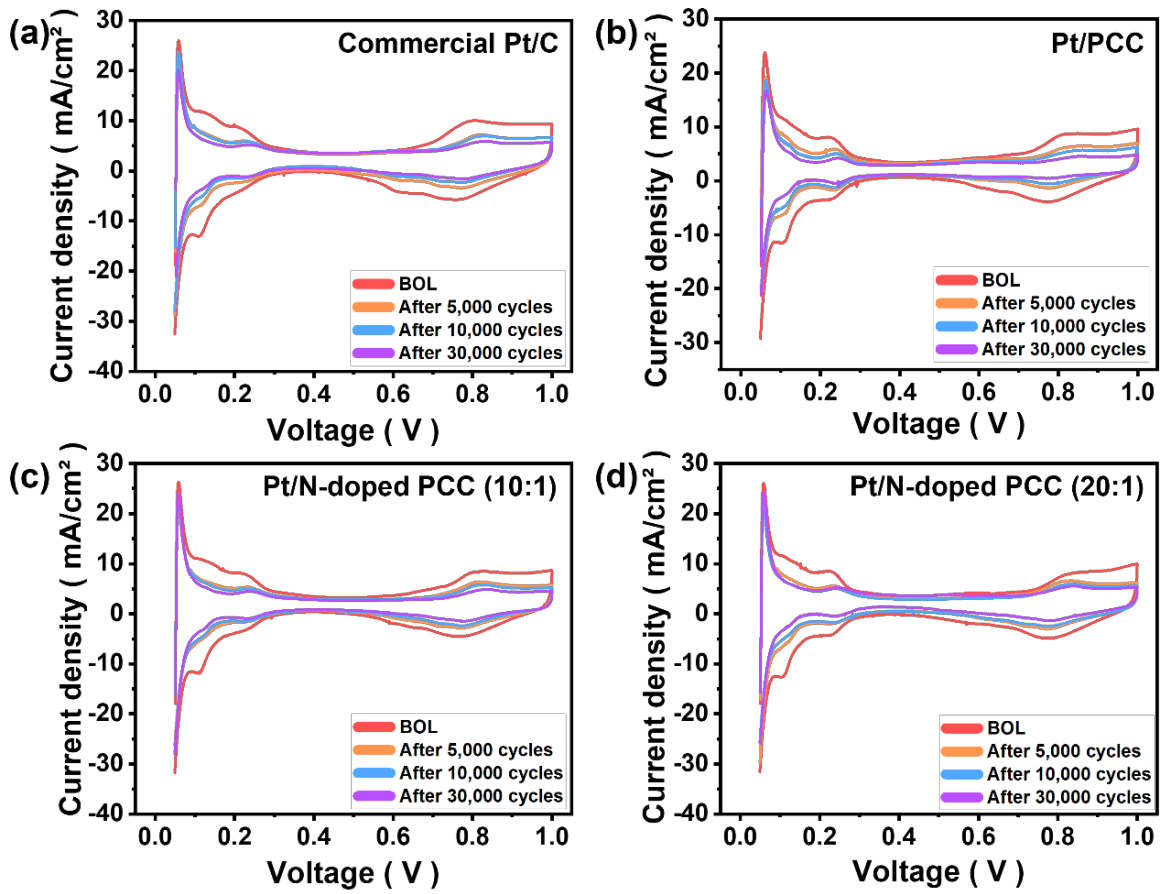

Fig. S14. CV curves of (a) commercial Pt/C, (b) Pt/PCC, (c) Pt/N-doped PCC (10:1), and (d) Pt/N-doped PCC (20:1). The curves are shown for BOL, after 5,000, after 10,000, and after 30,000 cycles under 100% RH.

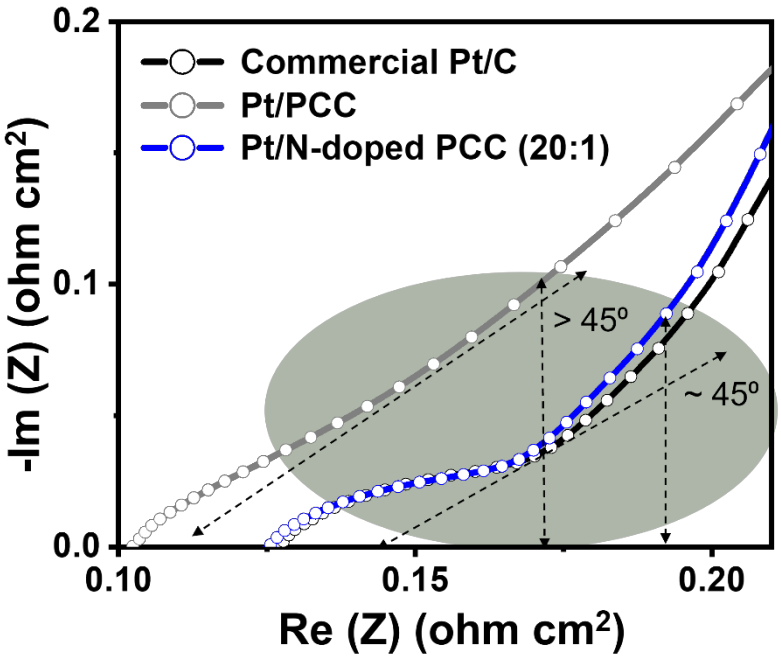

Fig. S15. EIS spectra of MEAs employing Pt/N-doped PCC (20:1), Pt/PCC, and commercial Pt/C as cathode catalysts, with commercial Pt/C as the anode under single-cell operation.